Controlling chaos in low- and high-dimensional systems with periodic parametric perturbations

K. A. Mirus and J. C. Sprott
Department of Physics, University of Wisconsin, Madison, Wisconsin 53706
(Received 29 June 1998)

The effect of applying a periodic perturbation to an accessible parameter of various chaotic systems is examined. Numerical results indicate that perturbation frequencies near the natural frequencies of the unstable periodic orbits of the chaotic systems can result in limit cycles for relatively small perturbations. Such perturbations can also control or significantly reduce the dimension of high-dimensional systems. Initial application to the control of fluctuations in a prototypical magnetic fusion plasma device will be reviewed. [S1063-651X(99)11505-8]

PACS number(s): 05.45.−a, 47.52.+j, 52.35.Mw, 52.55.Hc

I. INTRODUCTION

Since the pioneering work of Ott, Grebogi, and Yorke (OGY) in controlling chaotic systems [1], several other methods for controlling chaos [2–18] have evolved based on the principle that relatively small perturbations to a chaotic system can stabilize unstable periodic orbits (UPO's) possessed by that system. Such control schemes are attractive for two reasons. First, since chaotic systems possess an infinite number of unstable periodic orbits, a single physical system can exhibit a wide variety of controlled behaviors. Second, since the schemes are based on very general properties of chaotic dynamics, they are applicable to a wide variety of seemingly unrelated physical systems. Control methods inspired by the OGY method tend to be ''closed-loop'' control systems in which the applied perturbation is determined by the state of the system. There also exist ''open-loop'' control systems [19] in which the applied perturbation is independent of the system's state; that is, there is no feedback loop. Such control schemes involved modulating the chaotic systems with random [20–25], chaotic [26–28], or periodic signals [29–48].

Here the open-loop control scheme of applying a periodic perturbation to an accessible system parameter is examined for several different chaotic systems of increasing dimension and realism. Previous work has focused on the effect of a single periodic perturbation to a single system. Here, we demonstrate the general effects of periodic perturbations on a wide variety of systems. The numerical systems that have been examined are the logistic equation (a one-dimensional quadratic map), the Lorenz equations (a three-dimensional quadratic flow), the Rössler equations (another three-dimensional quadratic flow), a coupled Lorenz cell model (a 96-dimensional polynomial flow), the Yoshida equations, which a model magnetic fluctuations in a plasma fusion device (a nine-dimensional polynomial flow), and a neural net model for a fluctuating plasma (a 64-dimensional nonlinear map). Initial attempts to control magnetic fluctuations in the Madison Symmetric Torus (MST) [49] will also be mentioned.

In applying these perturbations, drive frequencies were sought for which a small amplitude would suffice to decrease the chaos in the system over a range of its parameters. Previous work found successful perturbation frequencies to be rational multiples of periodic drive frequencies that initiated the chaos [36–45], the natural frequencies in a period-doubling route to chaos [46], or frequencies corresponding to peaks in the power spectrum [47,48]. However, it will be shown that these predictors are not always reliable. Rather, the optimum perturbation frequencies correspond to rational multiples of the frequencies of UPO's embedded in the attractor. These UPO's can be extracted directly from the time series of any state-space variable, and thus no model for the system dynamics is required to predict optimum perturbation frequencies.

In this study, the Lyapunov dimension is computed to determine the effect of the applied perturbations. The Kaplan-Yorke conjecture [50–52] states that for an N-dimensional system, the Lyapunov dimension, which is an approximation to the information dimension, can be computed from the spectrum of Lyapunov exponents $(\lambda_1,\ldots,\lambda_N)$ when they are ordered from most positive to most negative. The first exponent in the spectrum, λ_1, or the largest Lyapunov exponent (LLE), can be used by itself to diagnose whether a system is chaotic or not. However, an applied perturbation may decrease the dimension of a system without making the system periodic. The Lyapunov dimension provides a means of diagnosing this effect on high-dimensional numerical systems, which would be impossible with more traditional time-series analysis. Note that applying a periodic perturbation increases the dimension of the system by one, because an extra state-space variable is added to the system. The Lyapunov exponent associated with this new state-space variable is always zero, because it causes neither exponential expansion nor contraction. It is not necessarily obvious that adding an external frequency to a system with an already broadband frequency spectrum will decrease its chaotic behavior, especially since three incommensurate frequencies can generally lead to chaos [53].

II. THE LOGISTIC EQUATION

The logistic equation is a well-known one-dimensional map with the following form:

$$x_{n+1}=ax_n(1-x_n). \tag{1}$$

The controlling periodic perturbation was taken as $a=a_0+a_1\cos(2\pi n/T+\varphi)$.

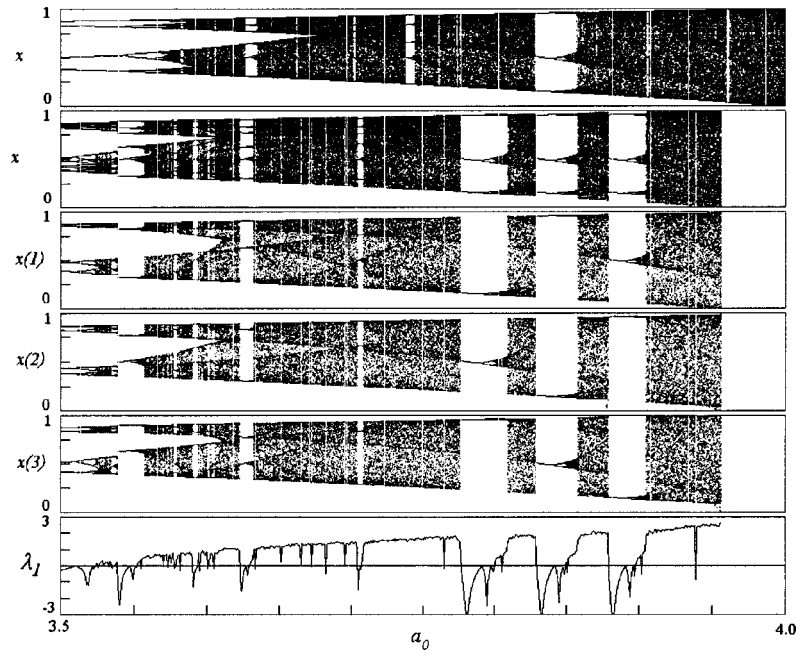

FIG. 1. Logistic map bifurcation diagram for a $T=3$ perturbation with $a_1=0.05$ and $\varphi=\pi/2$, showing the unperturbed bifurcation diagram, the perturbed map, its three composed maps, and the Lyapunov exponent.

To compute the Lyapunov exponent spectrum for the perturbed map, one can make it autonomous by splitting the map into two maps, with ''time'' represented by the second map. Letting $x_n(1)$and $x_n(2)$ denote the two state-space variables at iteration n, the maps take the following form:

$$x_{n+1}(1)=\{a_0+a_1\cos[2\pi x_n(2)/T+\varphi]\}x_n(1)[1-x_n(1)],$$
$$x_{n+1}(2)=x_n(2)+1. \tag{2}$$

An explicit computation of the Jacobian for these two maps shows that the two Lyapunov exponents are given by

$$\lambda_1=\lim_{N\to\infty}\frac{1}{N}\sum_{n=1}^{N}\ln\left|\left[a_0+a_1\cos\left(\frac{2\pi x_n(2)}{T}+\varphi\right)\right]\times[1-2x_n(1)]\right|,$$
$$\lambda_2=\lim_{N\to\infty}\frac{1}{N}\sum_{n=1}^{N}\ln|1|=0. \tag{3}$$

Since λ_2 is identically zero, calculation of λ_1 suffices to quantify the chaos. Previous analytic work [29–33] has lifted the nonautonomy by examining p composite maps formed from the pth iterate maps for a period-p perturbation.

The choice of the period of the perturbation is simple, since the logistic map has unstable orbits of all integer periods, provided the parameter a is large enough. In fact, there are 2^p unstable periodic orbits for any UPO of periodicity p when $a=4$ [54]. Most of the literature has focused on low-period perturbations. Here we will illustrate that control can be achieved for a period-three perturbation and that a perturbation that does not correspond to any UPO can obliterate all periodic windows.

A period-three drive results in the following two equivalent autonomous systems:

$$x_{n+1}(1)=\{a_0+a_1\cos[(2\pi/3)x_n(2)+\varphi]\}x_n(1)[1-x_n(1)],$$
$$x_{n+1}(2)=x_n(2)+1, \tag{4}$$

$$\begin{aligned}x_{n+1}(i)=&-A_iA_{i+1}^4A_{i+2}^2x_n(i)^8+4A_iA_{i+1}^4A_{i+2}^2x_n(i)^7\\&-2A_iA_{i+1}^3A_{i+2}^2(3A_{i+1}+1)x_n(i)^6+2A_iA_{i+1}^3A_{i+2}^2(2A_{i+1}+3)x_n(i)^5\\&-A_iA_{i+1}^2A_{i+2}(A_{i+1}^2A_{i+2}+6A_{i+1}A_{i+2}+A_{i+2}+1)x_n(i)^4\\&+A_iA_{i+1}^2A_{i+2}(A_{i+1}A_{i+2}+A_{i+2}+1)x_n(i)^3\\&-A_iA_{i+1}A_{i+2}(A_{i+1}A_{i+2}+A_{i+1}+1)x_n(i)^2+A_iA_{i+1}A_{i+2}x_n(i),\end{aligned} \tag{5}$$

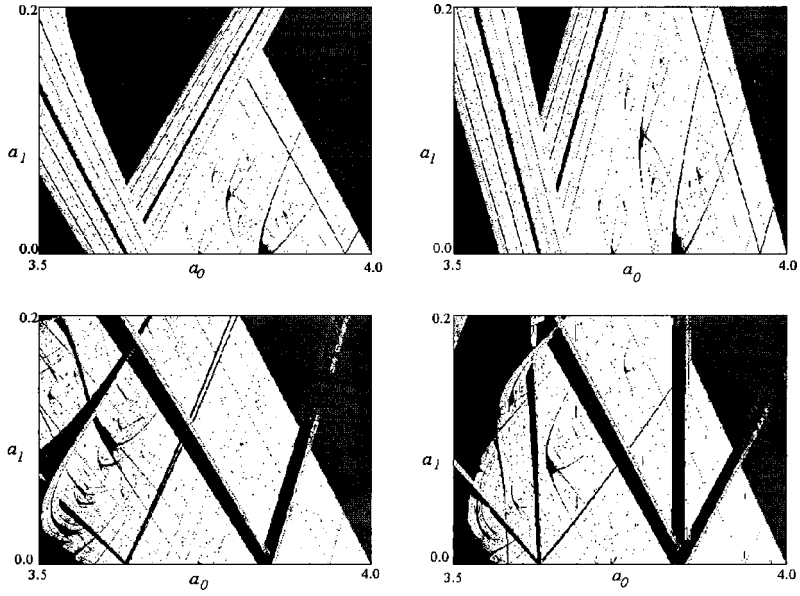

FIG. 2. Summary of effects of $T=2$ and 3 perturbations on the logistic map over a range of nominal parameter values a_0 and perturbations amplitudes a_1 for different phases. Clockwise, from upper left: $T=2$, $\varphi=0$; $T=2$, $\varphi=\pi/3$; $T=3$, $\varphi=\pi/2$; $T=3$, $\varphi=0$. Black indicates periodic solutions; white chaotic solutions, and gray unbounded solutions.

where the A_i are cyclic on (1,2,3) and $A_1=a_0+a_1\cos(\varphi)$, $A_2=a_0+a_1\cos(2\pi/3+\varphi)$, and $A_3=a_0+a_1\cos(4\pi/3+\varphi)$. Figure 1 shows the bifurcation diagram for the $T=3$ case. In this case, the period-three limit cycle window, which for the unperturbed case starts at $a=1+\sqrt{8}$, is triplicated, and its stability range is extended to values less than $1+\sqrt{8}$, as has the range of a_0, for which limit cycles with periods that are multiples of three have been extended.

Figure 2 answers the question of whether a perturbation can decrease the overall chaos for a nonlinear system over a broad range of parameters. It shows the effect of perturbing the logistic map with a $T=2$ and with a $T=3$ perturbation with $3.5<a_0<4$ and $0<a_1<0.2$ for two different phases φ. For $T=2$ and $\varphi=0$, the percentage of periodic cases was increased from 22.3% to 24.9% over this range of a_0 and a_1. The $T=2$, $\varphi=\pi/3$ case decreases the periodic solutions from 22.3% to 12.8%. A difference due to phase can also be seen in the $T=3$ cases. For $\varphi=\pi/2$, the number of periodic cases is increased to 26.9%, while for $\varphi=0$, the number is decreased to 16.2%. The effect of the phase φ is also manifested by the loss of the ''middle periodic ray'' when $\varphi=0$, because the logistic map is only being perturbed with two different perturbation amplitudes: a_1 and $-a_1/2$. Patterns similar to those in Fig. 2 were first examined by Markus, who varied the logistic equation parameter according to various symbolic sequences [55].

The result of perturbing the logistic map with a non-UPO period is shown in Fig. 3. The only ''off-resonance'' perturbations that can be applied are those with irrational periods to the limits of computational precision. Figure 3 shows that a maximally irrational period of $T=3+(\sqrt{5}-1)/2$ (the golden mean above 3) with $a_1=0.05$ destroys the periodic

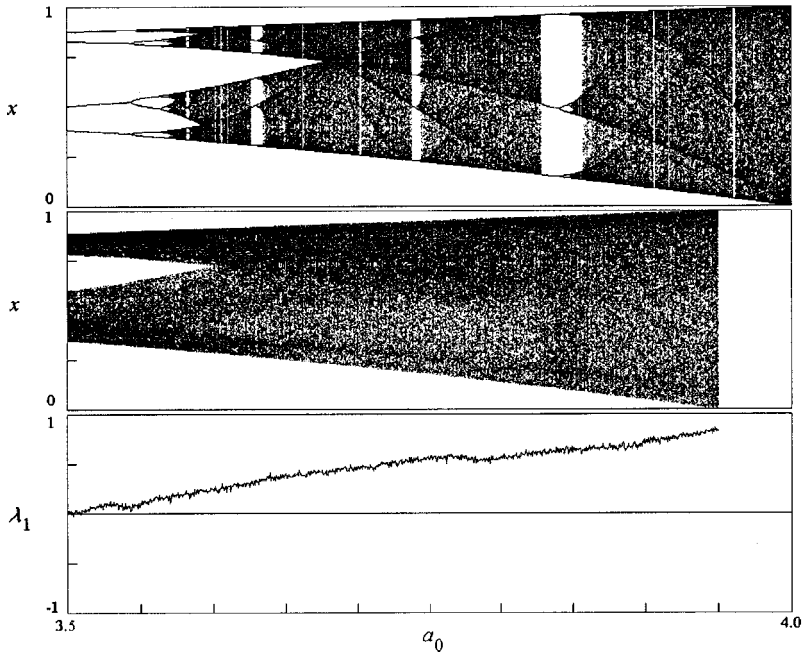

FIG. 3. Effect on the logistic map of a $T=3+(\sqrt{5}-1)/2$ perturbation for $a_1=0.05$; all periodic windows are destroyed.

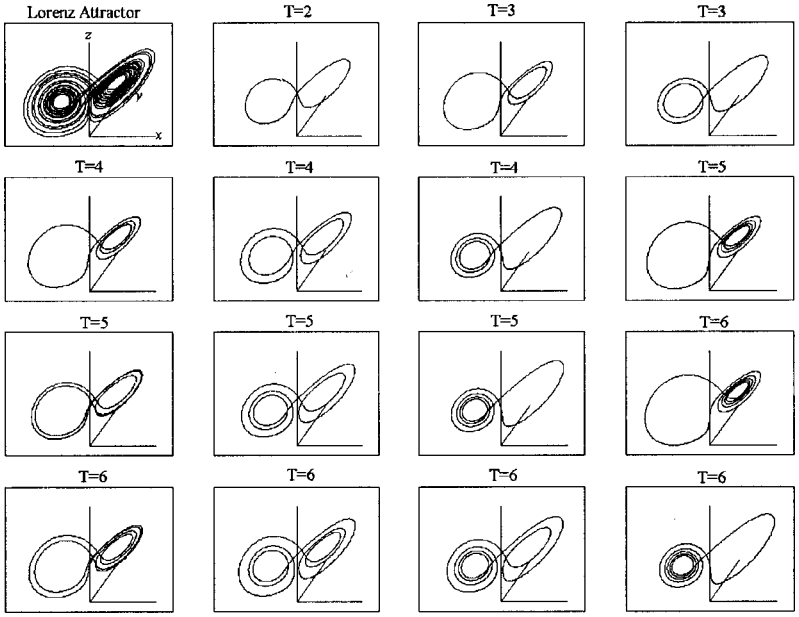

FIG. 4. The Lorenz attractor and its first six UPO's.

windows. The opening of periodic windows with resonant-perturbations and their closing with nonresonant perturbations is a general feature of all the systems studied here.

III. THE LORENZ EQUATIONS

The Lorenz equations [56] specify a three-dimensional flow given by the following equations:

$$\dot{x} = \sigma(y - x),$$
$$\dot{x} = x(r - z) - y, \tag{6}$$
$$\dot{z} = xy - bz.$$

Here the parameters $\sigma = 16, r = 45.92$, and $b = 4$ were used. In this and the remaining cases, all differential equations were integrated with a fourth-order Runge-Kutta method with a fixed step size, except where noted. Lorenz derived these equations to model heat convection in a Bénard convection cell, which consists of two horizontal, infinite plates with a temperature difference of ΔT across the fluid between the plates. After truncation of the fluid equations and renormalization of several of the fluid quantities, the parameter r is proportional to the temperature difference. Thus, in the spirit of perturbing a physically accessible system parameter, the parameter r was perturbed according to $r = r_0 + r_1 \sin(\omega t)$. Note that a fixed-point solution is not possible unless $\omega = 0$ or $r_1 = 0$.

The perturbation frequency is chosen by identifying the UPO's using a slight variation of the method of Lathrop and Kostelich [57]. In their work, UPO's are identified from a time series by reconstructing the attractor with time delays and then measuring the number of time steps it takes for the trajectory to return to within a distance ε of any given point. A suitable value for ε is found to be roughly a factor of 2 larger than the average state-space distance between successive points on the reconstructed attractor. If a given starting point on the trajectory returns to within ε of itself after m steps, it is called an (m,ε) recurrence point. When the $\{m\}$ for all (m,ε) recurrent points are histogrammed, the data cluster in integer multiples of Δm. When this method was applied to the Lorenz equations, it was found that $\Delta m = 124 \pm 9$, which for a time step of 1/256 corresponds to a temporal value of 0.48 ± 0.04. This method can also be applied to the three state-space variables (x,y,z) to find (m,ε) recurrent points. This method gives $\Delta m = 238 \pm 10$, which for a time step of 1/512 corresponds to 0.46 ± 0.02, which is in excellent agreement with the Lathrop-Kostelich method. The UPO's found using all three state-space variables bear a striking resemblance to the Lorenz attractor, as can be seen in Fig. 4. Note that for any given period T, there are $T-1$ distinct UPO's for the Lorenz attractor. Figure 5 shows the (m,ε) histogram obtained using this method.

A third method to find UPO's was used to verify the previous two results. Since the Lorenz attractor is low dimensional ($D_{KY} \cong 2.07$ for these parameters), a Poincaré map can be used to determine the periods of the UPO's. Both of the values of the state-space variables x and $\phi\,(=\omega t)$ are recorded when the attractor trajectory crosses the plane $z = r - 1$, which contains two of the fixed points of the unperturbed attractor. If the elements of the time series for x that

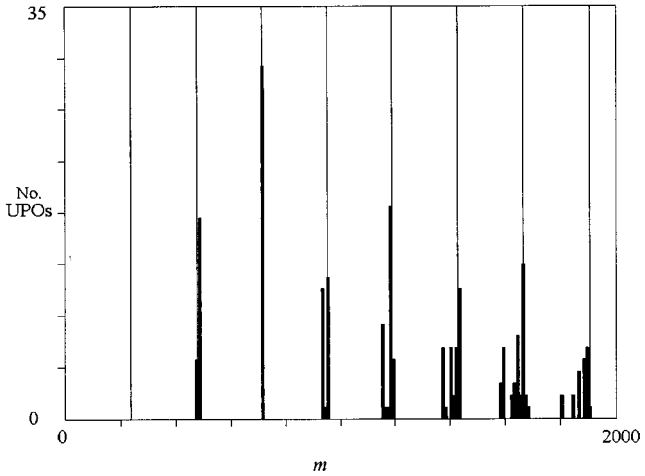

FIG. 5. Histogram of the number of UPO's with recurrence time m for the Lorenz equations. The vertical lines are spaced at $\Delta m = 238$.

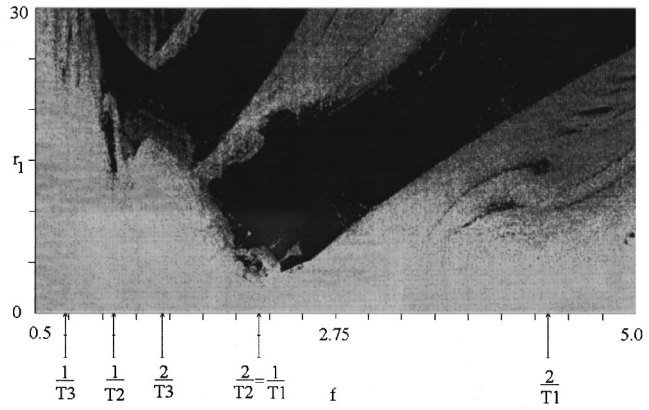

FIG. 6. Results of perturbing the Lorenz equations with various perturbations of frequency f and amplitude r_1. Arrows denote various UPO frequencies (i.e., $T2$ corresponds to a period-two UPO) and their harmonics. Black $\rightarrow$ periodic, dark gray $\rightarrow 2<D_{\mathrm{KY}}<3$, and light gray $\rightarrow\ 3<D_{\mathrm{KY}}<4$.

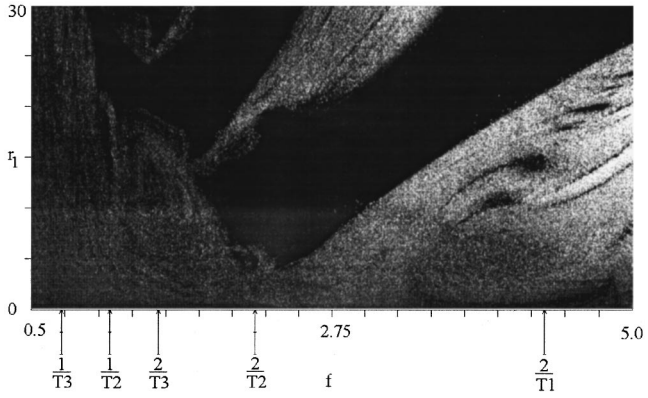

FIG. 7. Largest Lyapunov exponent for the perturbed Lorenz equations. Black corresponds to a LLE of 0; lighter colors indicate higher LLE's. The arrows indicate the same frequencies as in Fig. 6.

results are denoted as x_n, the intersection of the 45° line with plots of x_{n+k} vs x_n denotes UPO's of period $k/2$, and the temporal value of this period can be obtained from ϕ. This analysis gave a value of 0.46 ± 0.03, which agrees well with the values previously obtained.

To understand the stabilizing effect of periodic perturbations on the Lorenz equations, numerous perturbation frequencies and amplitudes were examined. Frequencies ranging from 0.5 to 5.0 Hz were used, which corresponds to just less than the frequency of a period-four UPO to four times the frequency of a period-two UPO. Amplitudes up to 66% of r_0 were used. For σ and b held constant as prescribed above, the Lorenz equations are chaotic from $r\approx31.375$ to $r>100$. Thus, the largest amplitude perturbations ($r_1=30.25$) bring the perturbed parameter $r=45.92+r_1\sin(\omega t)$ into a periodic regime for part of the drive period. However, many stabilizing amplitudes were too small to do this. Combinations of driving amplitude r_1 and frequency $f=\omega/2\pi$ were raster scanned, and the results were classified according to the Lyapunov dimension of the resulting perturbed attractor in Fig. 6. The dominant feature is a reduction in dimension at frequencies corresponding to the UPO's and their multiples. Note that the dimension of the system immediately increased by 1.0 when arbitrarily small perturbations r_1 were applied.

Figure 7 shows that the behavior of D_{KY} is replicated with the LLE, which is computationally easier to determine in general. Figure 8 shows some of the UPO's that were stabilized with small perturbations. The fluctuation amplitudes are decreased for cases controlled with small perturbations, since the attractor is confined to a smaller region of state space. For large perturbations, however, the fluctuation amplitudes increased, since the attractor size scales roughly linearly with r.

One surprising discovery was that the frequency of the perturbation that stabilizes a given UPO in the Lorenz attractor is rarely the natural frequency of that UPO. For example, a period-two UPO with a natural frequency of 1.1 Hz is commonly stabilized by a perturbation frequency of $\sim$2.2 Hz. This result is typical in that the smallest frequency usually required to stabilize a given UPO is twice its natural frequency or more, and it may occur because the period-one UPO for the Lorenz equations does not exist. However, the stabilized $T=3$ UPO in the upper right-hand corner of Fig. 8 provides one counterexample, since a period-three UPO is stabilized by a frequency that is closest to that of the nonexistent period-one UPO. Another typical occurrence is that a given perturbation frequency may stabilize several different UPO's. Figure 9 shows four such cases in which a period-one frequency aliases a period-four and period-eight UPO, a period-two frequency aliases a period-sixteen UPO, and twice a period-one frequency aliases a period-twelve UPO. It is also interesting that the width of effective perturbations in frequency gets narrower as higher-order UPO's are stabilized, and that these higher-order UPO's require larger perturbation amplitudes to stabilize them. Once any of the UPO's are stabilized, however, they remain controlled for as long as the perturbation is on.

Another unanticipated result is that as the amplitude of the perturbation is increased at a fixed frequency, the system can pass through regimes of control and chaos. Control with small perturbations happens only near natural frequencies of various UPO's, but as the amplitude is increased, chaotic and

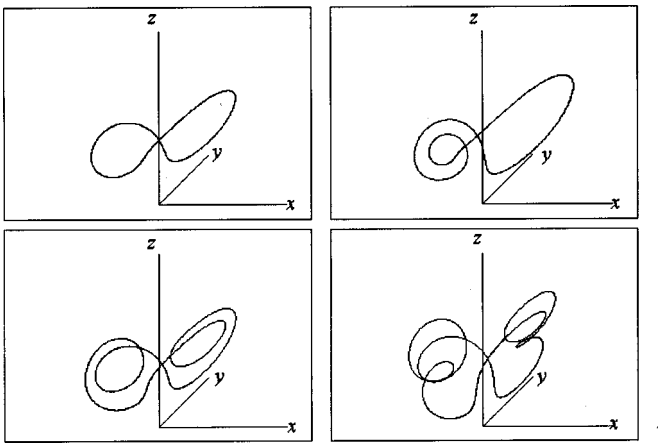

FIG. 8. Various stabilized UPO's for the perturbed Lorenz equations. clockwise, from upper left corner: period 2, $(r_1,f)=(4,2.412)$; period 3, $(r_1,f)=(3.375,2.072)$; period 6, $(r_1,f)=(23,0.712)$; period 4, $(r_1,f)=(13,1.108)$.

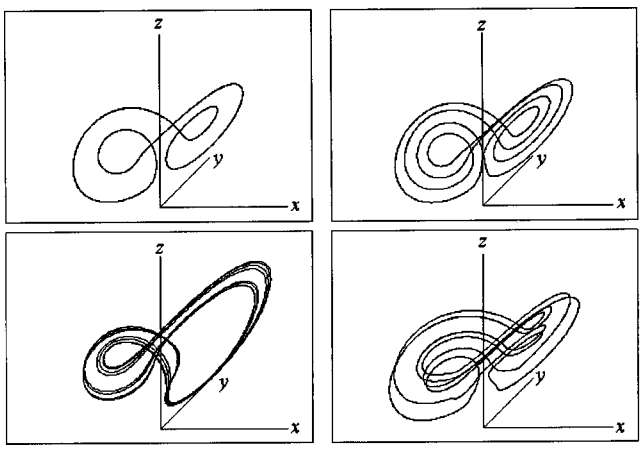

FIG. 9. Some ''aliased'' UPO's. Clockwise, from upper left corner: period 4, $(r_1,f)=(4.25,2.204)$; period 8, $(r_1,f)=(4.125,2.156)$; period 12, $(r_1,f)=(18.625,4.624)$; period 16, $(r_1,f)=(22.750,0.992)$.

periodic windows appear. The second band of periodicity (in the region $1<f<2.5$ and $r_1>15$ of Fig. 6) corresponds to a situation where the amplitude of the drive is so great that the system is mode locked to the perturbation. In this and similar cases, the limit cycles no longer resemble any unperturbed UPO but are akin to the top two plots in Fig. 10. This increasing distortion of the underlying attractor with larger perturbations is a common effect even for frequencies that stabilize a natural UPO.

The choice of initial condition can lead to differing results, as seen in the bottom two plots of Fig. 10. Although the specific details of a trajectory like this can be different for different initial conditions, no cases were found in which different initial conditions led to totally different behavior, such as the stabilization of different UPO's.

In addition to these results, some long-period limit cycles and unique strange attractors were also seen. Frequently, when a perturbation is applied, a chaotic attractor results, except that the chaos is limited to a thin band around some

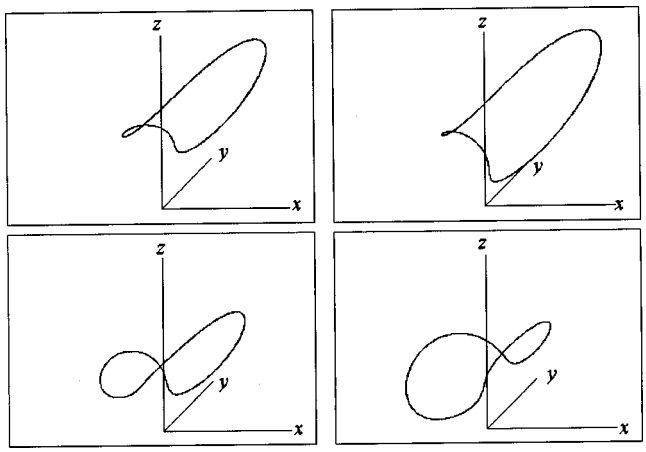

FIG. 10. Top two plots: limit cycle achieved through mode locking; $(r_1,f)=(25,2.176)$ (left), $(r_1,f)=(22,1.2)$ (right). Bottom two plots: slightly different period-two IUPO's, both stabilized with $(r_1,f)=(4.75,2.328)$ but different initial conditions: $(x_0,y_0,z_0,\phi_0)=(1,1,1,0)$ (left); $(x_0,y_0,z_0,\phi_0)=(1,1,10,0)$ (right).

UPO. This effect was termed ''noisy periodicity'' by Lorenz [58], and if there is room for some tolerance in the periodic solution that is sought, these solutions may suffice.

As with the logistic equation, small periodic perturbations stabilize the Lorenz equations when applied at frequencies near the natural frequencies of UPO's. Once a limit cycle is achieved, it remains stable for as long as the perturbation is on. Large perturbations stabilize the Lorenz equations by mode locking (stabilizing a highly distorted UPO). It should be noted that Singe *et al.* [59] were successful at controlling the Lorenz equations both numerically and experimentally in a system known as a thermal convection loop. Their method was simpler than the OGY method in that they used a simple proportional feedback scheme. The advantage of the method presented here is that it is even simpler because it involves no feedback whatsoever. A disadvantage of this method is that it is impossible to stabilize fixed points in the chaotic system.

IV. THE RÖSSLER EQUATIONS

The Rössler equations [60] are

$$\dot{x}=-(y+z),$$

$$\dot{y}=x+ay, \tag{7}$$

$$\dot{z}=b+z(x-c).$$

Here, the parameters $a=b=0.2$ and $c=5.7$ were used. Rössler derived these equations as a simpler example than the Lorenz equations in the sense that they have only one quadratic nonlinearity, and the flow they generate has only a single spiral (see the attractor in the upper left of Fig. 12). See Sprott [61–63] for even simpler examples of chaotic flows. Although the Rössler equations have a simpler form than the Lorenz equations, they were found to be more difficult to control due to the presence of a dominant frequency. Since the Rössler equations and their parameters have no physical significance, the parameter c was chosen arbitrarily to be perturbed: $c=c_0+c_1\sin(\omega t)$. Analysis of 500 UPO's identified using the (m,ε) method on all three state-space variables determined that $\Delta m=1488\pm4$, which for a time step of 1/256 corresponds to 5.81 ± 0.09. A Poincaré analysis of the UPO's yielded a similar result of 5.86 ± 0.02.

To assess the effect of periodic perturbations on the Rössler equations, perturbation amplitudes and frequencies in the range $0<c_1<3.1$ and $0.05<f<0.4$ were examined, corresponding to amplitudes up to 54% of c_0 and frequencies of just less than that of a period-three UPO to more than twice the frequency of a period-one UPO. For a and b held constant as prescribed above, the Rössler equations are chaotic from $c\approx4.20$ to $c>13$. Thus, perturbation amplitudes greater than $c_1=1.5$ bring the perturbed parameter $c=5.7+c_1\sin(\omega t)$ into a periodic regime for part of the drive period. However, as was the case with the perturbed Lorenz equations, many stabilizing amplitudes were smaller than the $c_1=1.5$ limit. Figure 11 shows that perturbations near the UPO and its multiples decrease the dimension of the attractor. Figure 12 shows some of the UPO's that were stabilized with small perturbations, as well as a noisy limit cycle.

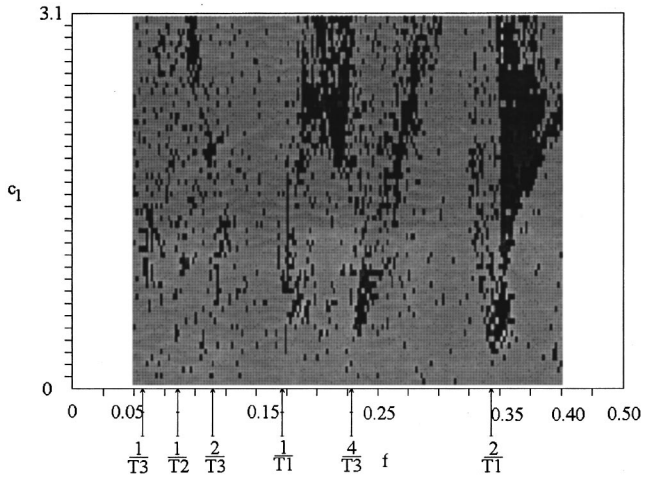

FIG. 11. Results of perturbing the Rössler equations. The arrows show the frequencies of various UPO's and their harmonics. Black → periodic, dark gray → $2<D_{KY}<3$, and light gray → $3<D_{KY}<4$.

V. COUPLED LORENZ EQUATIONS

Coupled Lorenz models are lattices with each site occupied by a set of Lorenz equations. Lawandy *et al.* [64] have studied pairs of coupled Lorenz systems in order to find an improved stability regime for a single-mode laser by coupling two lasers together. Malkus [65] and Yorke and Yorke [66] showed that the Lorenz equations, which were derived as an approximation of the Raleigh-Bénard system, exactly describe the dynamics of a thermal convection loop. A thermal convection loop, or thermosyphon, consists of a narrow diameter pipe containing fluid, which is bent into a torus, stood upright in a vertical plane, heated uniformly over the bottom half, and cooled uniformly over the top half. Davis and Roppo [67] studied the effect of thermally coupling two thermosyphons, which is equivalent to studying two adjacent rolls in a Bénard convection layer. Jackson and Kodogeorgiou [68] extended this work by studying long (up to 128 lattice sites) periodic chains of thermosyphons. They included both viscous and thermal coupling between adjacent vortices in their model equations but only examined the case with viscous coupling. Lorenz [69] also studied the effect of coupling seven Lorenz-like systems together to illustrate that global weather systems most likely do not possess low-dimensional attractors. Here the coupled Lorenz cell model studied by jackson and Kodogeorgiou is considered:

$$\dot{x}_i=\sigma(y_i-x_i)-\mu(x_{i+1}+x_{i-1}+2x_i),$$

$$\dot{y}_i=-y_i-x_iz_i+rx_i, \tag{8}$$

$$\dot{z}_i=x_iy_i-bz_i.$$

Here, i denotes the lattice site ($i=0,1,...,N-1$) and μ is the viscous coupling constant. Each lattice site is coupled to one neighbor on each side. This system is taken to have periodic boundary conditions: $x_N=x_0$, $y_N=y_0$, $z_N=z_0$. The parameters used here were $\sigma=10$, $\mu=3$, $r=34$, $b=1$, and $N=32$. In the thermosyphon paradigm, x corresponds to the average fluid velocity around the loop, y corresponds to the temperature difference between points at ''12 o'clock'' and ''6 o'clock,'' and z corresponds to the horizontal temperature difference. The authors computed that the system has stable fixed points for $r<r_c=17.5$, and it was found that the system exhibits chaotic behavior for r down to about 23.

Computing the Lyapunov exponent is computationally intensive for high-dimensional chaotic systems, since the memory and time required both scale as N^2. For this reason, a lattice with only $N=32$ sites (and thus $3\times32=96$ vari-

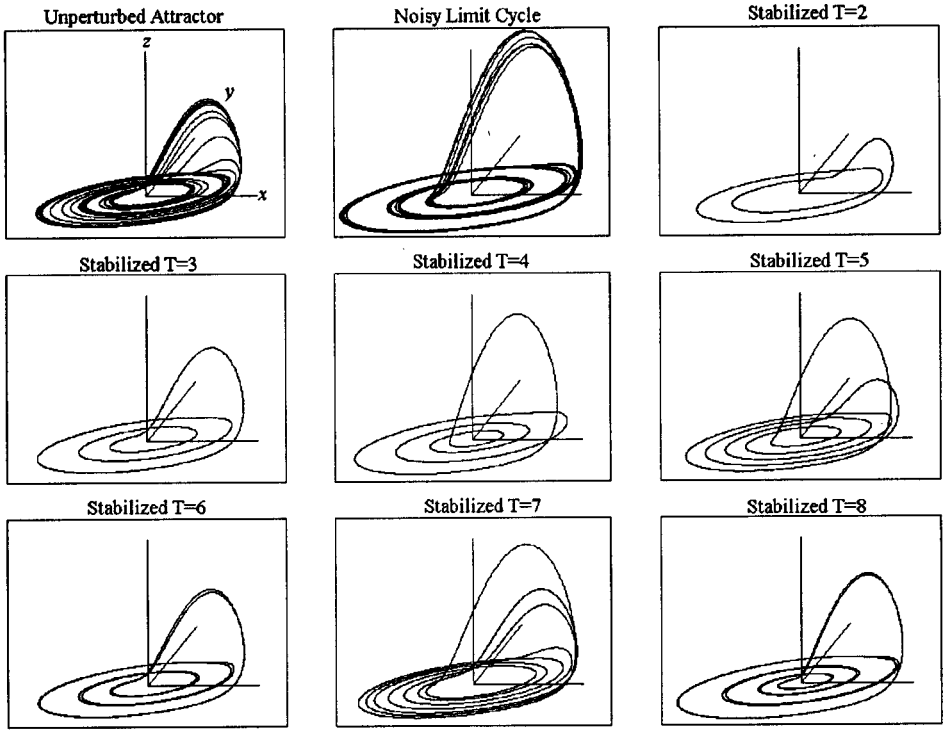

FIG. 12. Various attractors arising from the perturbed Rössler equations: The unperturbed Rössler attractor; a noisy $T=3$ limit cycle, $(c_1,f)=(1.600,0.182)$; a $T=2$ limit cycle, $(c_1,f)=(1.200,0.250)$; a $T=3$ limit cycle, $(c_1,f)=(0.100,0.114)$; a $T=4$ limit cycle, $(c_1,f)=(0.750,0.272)$; a $T=5$ limit cycle, $(c_1,f)=(0.450,0.106)$; a $T=6$ limit cycle, $(c_1,f)=(0.100,0.286)$; a $T=7$ limit cycle, $(c_1,f)=(1.050,0.356)$; a $T=8$ limit cycle, $(c_1,f)=(1.050,0.168)$.

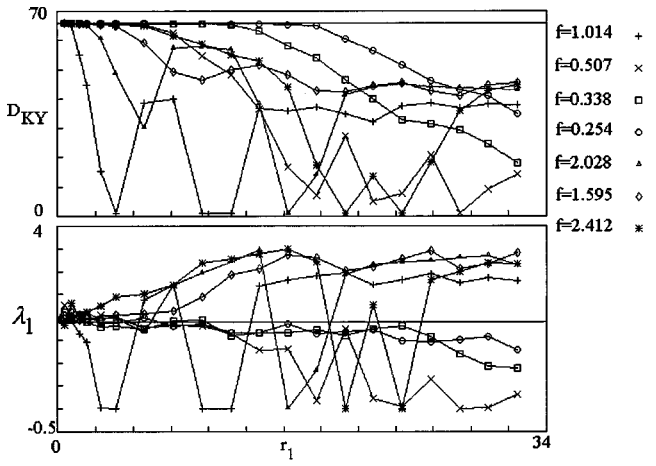

FIG. 13. Results of perturbing a coupled Lorenz system as evidenced by the Lyapunov dimension and the magnitude of the LLE. The solid horizontal lines indicate values for the unperturbed system. Note that a perturbation frequency $f=1.014$ produces a limit cycle for $r_1=4.0$, 10.0, and 12.0.

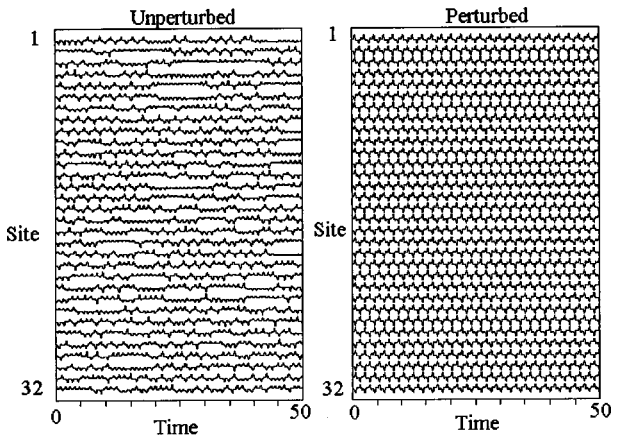

FIG. 14. Spatiotemporal plot of x_i vs time for the coupled Lorenz equations. Left: unperturbed; right: perturbation amplitude of $(r_1,f)=(4,1.014)$. The perturbed case is a period-two limit cycle.

ables) was considered, and a first-order ''leapfrog'' integration scheme was used. It was found that great care had to be used in choosing the integration time step so that the classical Gram-Schmit orthonormalization technique used for computing the Lyapunov exponent spectrum was numerically stable. In the absence of a perturbation, this 96-dimensional system has an attractor with a Lyapunov dimension of 65.8. The uncoupled Lorenz equations for these parameters were measured to have $D_{\mathrm{KY}}=2.06\pm0.005$, which yields an expected dimension for the coupled system of $32\times2.06=65.9$. This value is in good agreement with what was measured for the coupled system, although it would not have been surprising if the coupling had reduced the dimension. As with the single Lorenz model, the perturbed parameter was $r=r_0+r_1\sin(\omega t)$. A reasonably accurate calculation of D_{KY} for even this modest lattice size requires the order of a day of computation for one perturbation case. Thus, there are no extensive perturbation amplitude-frequency scans as before, but Fig. 13 shows the Lyapunov dimension and LLE as a function of perturbation amplitude for seven different perturbation frequencies.

The perturbation frequencies were once again chosen by identifying the frequencies of the UPO's for the coupled system. The period of the period-one UPO was found to be 1.014 ± 0.050. Remarkably, a small perturbation amplitude of $r_1=4$, which is only 9% the unperturbed value, resulted in limit-cycle behavior for a perturbation frequency equal to the frequency of a period-one UPO. Perturbations of frequency $f=2.028$ (which is twice the period-one UPO frequency) and $f=1.595$ (which is about three times the period-two UPO frequency) significantly decrease the dimension of the system. Even if a perturbation does not produce limit cycles, drastically decreasing the dimension of a high dimension system is a significant step toward controlling it [70]. Perturbations of frequency corresponding to a period-two ($f=0.507$), a period-three ($f=0.338$), and a period-four UPO ($f=0.254$) decrease the dimension of the system with respectively larger perturbations. A perturbation frequency of $f=2.412$, which was successful at eliminating chaos for the single Lorenz system, required a large amplitude to decrease the dimension of the system. None of the frequencies increased the dimension by more than 1, as has been seen with perturbed coupled logistic equations. Frequencies that are further off-resonance may excite additional, latent degrees of freedom. This case could have important applications in biological and other high-dimensional systems, where it is sometimes desirous to ''uncontrol'' chaos [71].

An important point in choosing the perturbation frequency for this case was that the frequency of the period-one UPO is roughly half the frequency of the power spectral peak of any single state-space variable. The power spectral peak occurs at roughly 2 Hz, which corresponds to the period-one UPO for a single Lorenz attractor. Thus, the global dynamics of the coupled system seem to evolve more slowly than the fluctuations in any state-space variable. This implies that the power spectral peak frequency is misleading when trying to predict a useful perturbation frequency for this system. The slower global dynamics are shown in spatiotemporal plots in Fig. 14, which shows the value of x_i, which corresponds to the average fluid velocity for each site versus time. The perturbed case in Fig. 14 shows the period-two limit cycle achieved with the small-amplitude period-one perturbation.

This result is particularly encouraging in view of its simplicity when compared to other work in controlling high-dimensional systems. The earliest method advanced for controlling high-dimensional chaotic systems [7] was a straight application of the OGY method, and it proved to be cumbersome in application. Recent methods of controlling high-dimensional chaotic systems have focused on arrays of controllers that use an OGY-like method based only on local measurements [72], delayed oscillating feedback [73], or linear control laws optimized by placing the controllers according to the symmetry of the system [74,75]. While these methods are effective, the method presented here has the advantage that no feedback is required, in sharp contrast to feedback applied by a potentially large number of controllers. The only requirement is that there exists a suitable global parameter accessible for applying a periodic perturbation.

VI. THE YOSHIDA EQUATIONS

The Yoshida equations are a set of ordinary differential equations derived by Yoshida *et al.* [76] from a 1D (i.e.,

functions have a radial dependence only) set of partial differential equations meant to model the nonlinear interactions of magnetic islands in a low-beta tokamak plasma in a cylindrical approximation. The method for reducing the (infinite-dimensional) set of PDE's to ODE's involves the application of the force-free condition $\nabla\times\mathbf{B}=\lambda\mathbf{B}$ to approximate the structure of the magnetic field $\mathbf{B}=\mathbf{B}_0+\mathbf{b}$. The nonlinear interactions are represented by fluctuations in the radial magnetic field (b_r), the poloidal magnetic field (b_θ), and the normalized parallel current density (λ).

The force-free condition converts PDE's to ODE's by reducing the action of spatial derivatives to the multiplication by a scalar function λ. The justification for the force-free structure of the field is that the intensity growth rate is sufficiently small that the current perpendicular to the magnetic field is negligible, which is indeed the case for a tokamak plasma in which the parallel current is significantly larger than any perpendicular currents. In the case of a reversed-field pinch plasma confined by a perfectly conducting toroidal shell, the relaxed state is defined by the force-free condition [77].

By combining the time evolution of the magnetic field, the time evolution of the magnetic helicity, and a hyperresistivity added to Ohm's law to describe the effect of the nonlinear coupling of the tearing modes, Yoshida *et al.* obtained the following set of three ODE's for each interacting island in a plasma:

$$\dot{b}_{r,n}=-\frac{\eta}{\mu_0}\lambda_n^2 b_{r,n}-V\lambda_n b_{\theta,n},$$

$$\dot{b}_{\theta,n}=-\frac{\eta}{\mu_0}\lambda_n^2 b_{\theta,n}+V\lambda_n b_{r,n}+\frac{C}{B_0}\frac{b_{r,n+1}+b_{\theta,n+1}^2-(b_{r,n-1}^2+b_{\theta,n-1}^2)}{\Delta_n}\times\frac{\lambda_{n+1}+\lambda_{n-1}-2\lambda_n}{\Delta_n^2},\tag{9}$$

$$\dot{\lambda}_n=\lambda_n^2\left[\frac{C}{2B_0^2}(b_{r,n}^2+b_{\theta,n}^2)\left(\frac{\lambda_{n+1}+\lambda_{n-1}-2\lambda_n}{\Delta_n^2}\right)+\frac{E_h}{B_0}\right].$$

Here, $b_{r,n}$, $b_{\theta,n}$, and λ_n are, respectively, the radial magnetic field fluctuation, the poloidal magnetic field fluctuation, and the parallel current density at a radial grid point indexed by n. η is the resistivity, μ_0 is the permeability of free space, V is the Hall velocity, C is a constant proportional to the tearing mode growth rate, B_0 is the equilibrium axial magnetic field, Δ_n is the distance between the $n-1$ and $n+1$ grid points, and E_h is the axial electric field used to drive the plasma current. The parameter E_h was chosen to be perturbed, since it is an accessible experimental parameter.

Yoshida *et al.* used these equations to model equally spaced two-mode interactions ($N=2$) in a tokamak plasma. This two-mode model was successfully controlled with periodic perturbations, but a three-mode model was sought that would describe an MST-like plasma [49] more accurately.

Modifying the Yoshida equations to model MST involves changing some of the boundary conditions, and accounting for the fact that bispectral analysis of experimental data reveals a three-wave coupling process, whereby two modes couple to a third with $k_3=k_1+k_2$ [78]. In MST, magnetic fluctuations are dominated by a few $m=1$ modes; namely $(m,n)=(1,6)$ and $(1,7)$. These two modes couple strongly to the (0,1) and (2,13) modes. The (0,1) mode is much more dominant than the (2,13) mode, but it is located at the reversal surface of the plasma, where the toroidal magnetic field vanishes. This violates the assumption of Yoshida *et al.* that the toroidal field is nearly constant across the plasma. However, the (2,13) mode lies between the (1,6) and (1,7) modes, which means the toroidal field is nearly constant across these three modes. Thus the (1,6), (2,13), and (1,7) modes were chosen to model the magnetic fluctuations in the MST. These modes are not equally spaced across the plasma. The (1,6), (2,13), and (1,7) modes reside approximately at $r/a=0.3$, 0.36, and 0.42, respectively. Incorporation of these modifications results in the following nine equations for this $N=3$ model:

$$\begin{aligned}
\dot{x}_1&=a_1x_1x_3^2+a_2x_2x_3,\\
\dot{x}_2&=a_1x_2x_3^2-a_2x_1x_3+a_3(x_4^2+x_5^2)(a_4-2x_3+x_6),\\
\dot{x}_3&=x_3^2[a_5(x_1^2+x_2^2)(a_4-2x_3+x_6)+a_6],\\
\dot{x}_4&=a_1x_4x_6^2+a_2x_5x_6,\\
\dot{x}_5&=a_1x_5x_6^2-a_2x_4x_6+0.833a_3(x_7^2+x_8^2-x_1^2-x_2^2)\\
&\quad\times(x_3-2x_6+x_9),\\
\dot{x}_6&=x_6^2[a_5(x_4^2+x_5^2)(x_3-2x_6+x_9)+a_6],\\
\dot{x}_7&=a_1x_7x_9^2+a_2x_8x_9,\\
\dot{x}_8&=a_1x_8x_9^2-a_2x_7x_9+0.714a_3(a_7-x_4^2-x_5^2)(x_6-2x_9),\\
\dot{x}_9&=x_9^2[a_5(x_7^2+x_8^2)(x_6-2x_9)+a_6].
\end{aligned}\tag{10}$$

Here, the parameter a_6 was perturbed, since it corresponds to the axial electric field E_h. Parameters chosen to give the best match between the autocorrelation functions of $\dot{x}_8$ and a single poloidal field pick-up coil on the wall of MST were $\{a_i\}=\{-0.578\,13,-1.7339,\ 9.781\,95,\ 0.668\,11,\ 5.465\,45,\ 0.661\,26,\ 3.639\,98\}$, with time in units of the digitization time of 5 μs. A comparison of the time series for MST data and the model equations is shown in Fig. 15. The period-one UPO had a temporal period of 15.8 ± 0.5. This corresponds to 79 ± 2.5 μs in the MST, which is a frequency of 12.7 ± 0.4 kHz. Like the coupled Lorenz equations, the period-one UPO has a frequency significantly lower than the peak power spectral frequency of 40 kHz. Figure 16 shows that the most effective controlling frequencies are the UPO frequencies and their harmonics rather than the peak power spectral frequency. An analysis of the electron heat transport due to radial magnetic field fluctuations in a Rechester-Rosenbluth model [79] showed only a slight ($\sim$10%) reduction for a perturbation at four times the period-one UPO frequency.

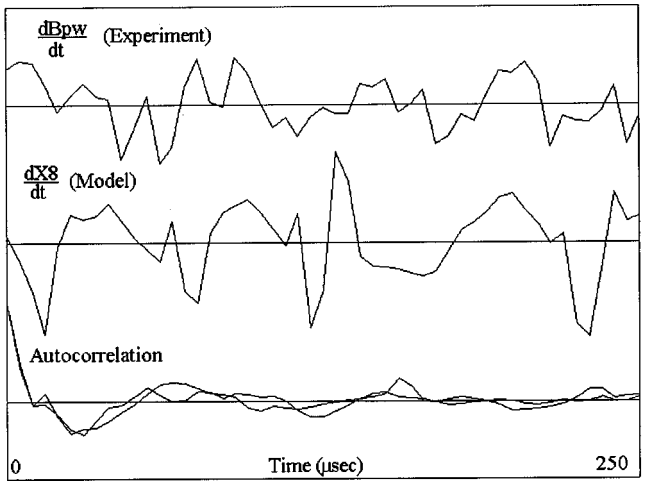

FIG. 15. A comparison of the measured poloidal field fluctuations at the wall of MST and from the outermost magnetic island in the $N=3$ Yoshida model. The bottom plot shows the autocorrelation function for the two signals.

VII. A NEURAL NETWORK MODEL FOR MST

An artificial neural network model can also be used to study prospects for controlling fluctuations in MST. The neural net chosen has N neurons, with the input of each neuron consisting of the superposition of the weighted sum of the output of all the neurons (including itself). The neurons are represented by hyperbolic tangent squashing functions that provide the nonlinearity necessary for chaos:

$$x_i(t+1)=\tanh\left(s\sum_{j=1}^{N} W_{ij}x_j(t)\right). \tag{11}$$

The parameter s is a scale factor on the weights and is initially chosen as $s=1$. The $N\times N$ matrix of weights W_{ij} is adjusted by a variant of simulated annealing so that the N outputs of the neurons $x_i(t+1)$ at T successive time steps fits an $N\times T$ matrix of training points obtained from an array of N poloidal field magnetic pickup coils (measuring dB_P/dt at the wall of MST). The training set has $N=64$ and $T=255$, with a sample time of 5 μs, and was rescaled so that the data fall in the range -1 to $+1$ as shown in Fig. 17. The dominant feature is a rotating resistive tearing mode with a frequency of about 14 kHz. After training the net for several days of 200 MHz CPU time, the output of the network captured some sense of the rotating mode seen in the experiment, with a frequency of about 11 kHz. The model was not chaotic, however, as evidenced by calculation of the LLE, which is indistinguishable from zero. To obtain a chaotic solution, the parameter s was increased to 1.2, giving the result in Fig. 18. This case has a largest Lyapunov exponent (base e) of 0.028/iteration. The rotating oscillation persists at a frequency of about 10 kHz. A perturbation $s=s_0+s_1\sin(2\pi ft)$ with $s_0=1.2$ was added, and the perturbation

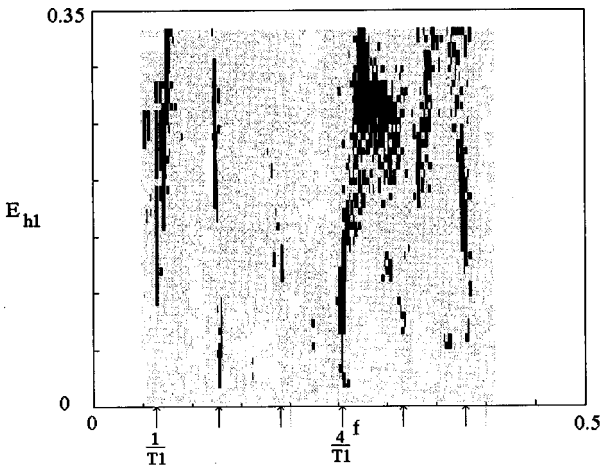

FIG. 16. Effect of perturbing the chaotic Yoshida equations modeling the MST The unperturbed parameter value was $a_6=E_{h1}\cong 0.66125$. Black indicates limit cycle cases. Dark gray $\rightarrow 2<D_{KY}<3$; light gray $\rightarrow 3<D_{KY}<4$; white $\rightarrow 4<D_{KY}<5$. The unperturbed case has a dimension of $D_{KY}=4.1$. The dark arrows indicate the frequency of the period-one UPO and its harmonics. The light gray arrows indicate the power spectral peak frequency and its harmonic.

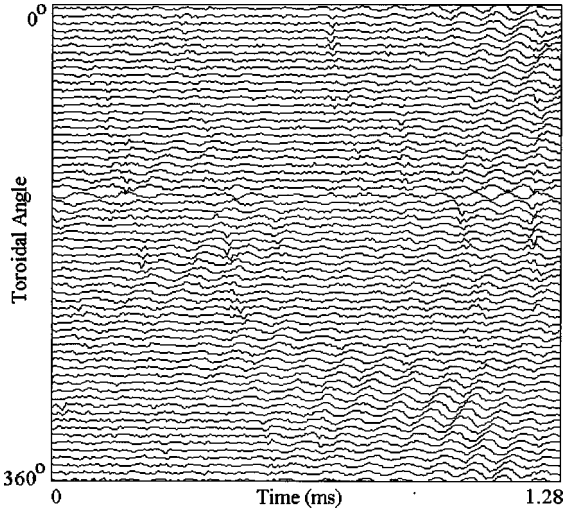

FIG. 17. Spatiotemporal plot of poloidal field fluctuations at the wall of MST. The dominant feature is a rotating resistive tearing mode with a frequency of about 14 kHz.

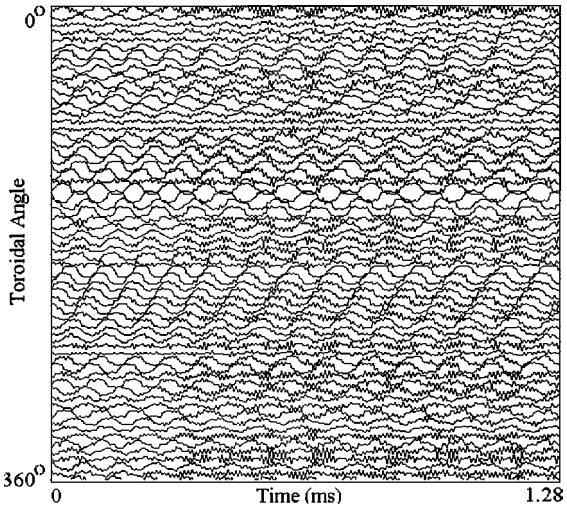

FIG. 18. Spatiotemporal plot of a neural network trained to model MST poloidal field fluctuations with the parameter s increased by 20% to yield chaotic solutions.

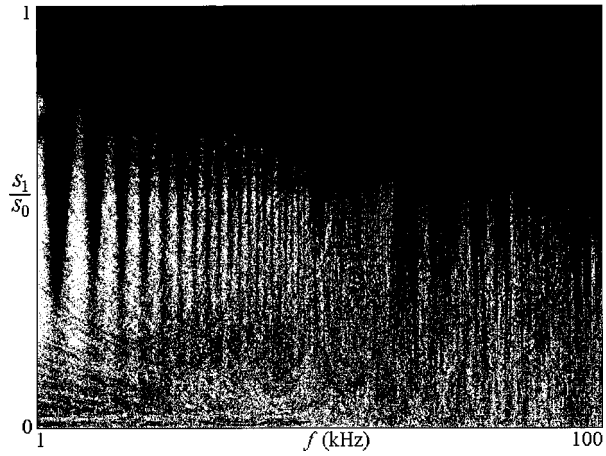

FIG. 19. Result of perturbing the chaotic MST neutral net model. Black indicates limit cycle behavior. White indicates the LLE was approximately doubled.

amplitude was scanned over the range $0<s_1<s_0$, while the frequency was scanned over the range $1<f<100$ kHz. The LLE was calculated for each combination of s_1 and f. The result is plotted in Fig. 19 with a gray scale in which the darkest color indicates an exponent of zero (chaos completely suppressed) and the lightest color indicates an enhancement of the chaos (approximate doubling of the Lyapunov exponent).

The general result is a decrease in chaos for increasing perturbation amplitude, with certain frequencies such as 13 kHz being especially effective. The striations in the upper left are a numerical artifact caused by truncating the calculation at a time (500 iterations) that is not an integer number of perturbations cycles. Since the Lyapunov exponent generally increases with s, chaos is enhanced when the final value of s is positive and diminished when it is negative for low perturbation frequencies.

VIII. PERIODIC PERTURBATIONS APPLIED TO MST

Periodic radial magnetic field perturbations (of a few tens of gauss) were applied to MST plasmas by driving a set of $n=1$ and 6 coil sets that pierced the toroidal gap. Calculations from magnetic fluctuation data show that the dominant UPO's for MST have a frequency of about 7 kHz, which is about half the peak power spectral frequency of the tearing modes. This result of the UPO having a slower time scale than is indicated by power spectra is consistent with numerical results for high-dimensional systems.

There is no evidence that the small periodic perturbations applied decreased the correlation dimension of the system ($D\geqslant 15$ [80]) to a level that could be measured. However, this result does not mean that they had no effect; rather that the effect could not be adequately diagnosed within the limits of the finite amount of noisy data. Higher-power experiments with better-tuned perturbations in the future may show positive effects, but it is uncertain if the perturbation can be properly tuned for each plasma shot, since UPO analysis indicated slight differences in the peak of the (m,ε) histogram from shot to shot. Also, numerical results suggest that the perturbation frequency has to be very close to the frequency of the UPO, and this frequency may change somewhat during and between shots.

IX. SUMMARY

Periodic perturbations have been applied to several chaotic numerical systems by modulating a system parameter. In every case, the optimum frequency to obtain control with a minimum perturbation amplitude was found to be the frequency of the UPO's obtained from the dynamical fluctuations of the system. One interesting result was that plots of controlled cases on a perturbation frequency-amplitude plane are dissimilar to the Arnold tongues [54,81] usually seen in systems that undergo a quasiperiodic route to chaos. This difference has been observed in at least one other experiment [43]. Also, a given frequency can stabilize more than one UPO. Another interesting discovery was that UPO's can have vastly different time scales than the fluctuations in a given state-space variable, which means that the best frequencies to perturb are not always those with the most power.

[1] E. Ott, C. Grebogi, and J. A. Yorke, Phys. Rev. Lett. **64**, 1196 (1990).
[2] W. L. Ditto, S. N. Rauseo, and M. L. Spano, Phys. Rev. Lett. **65**, 3211 (1990).
[3] P. M. Alsing, A. Gavrielides, and V. Kovanis, Phys. Rev. E **50**, 1968 (1994).
[4] U. Dressler and G. Nitsche, Phys. Rev. Lett. **68**, 1 (1992).
[5] B. Cazelles, G. Boudjema, and N. P. Chau, Phys. Lett. A **196**, 326 (1995).
[6] B. Hubinger, R. Doerner, W. Martienssen, M. Herdering, R. Pitka, and U. Dressler, Phys. Rev. E **50**, 932 (1994).
[7] D. Auerbach, C. Grebogi, E. Ott, and J. A. Yorke, Phys. Rev. Lett. **69**, 3479 (1992).
[8] T. Shinbrot, W. Ditto, C. Grebogi, E. Ott, M. Spano, and J. A. Yorke, Phys. Rev. Lett. **68**, 2863 (1992).
[9] E. R. Hunt, Phys. Rev. Lett. **67**, 1953 (1991).
[10] R. Roy, T. W. Murphy, Jr., T. D. Maier, Z. Gills, and E. R. Hunt, Phys. Rev. Lett. **68**, 1259 (1992).
[11] K. Pyragas, Phys. Lett. A **170**, 421 (1992).
[12] U. Dressler and G. Nitsche, Phys. Rev. Lett. **68**, 1 (1992).
[13] Y. Liu, L. C. Barbosa, and J. R. Leite, Phys. Lett. A **193**, 259 (1994).
[14] M. A. Matias and J. Guemez, Phys. Rev. Lett. **72**, 1455 (1994).
[15] Y. H. Chen and M. Y. Chou, Phys. Rev. E **50**, 2331 (1994).
[16] C.-C. Fuh and P.-C. Tung, Phys. Rev. Lett. **75**, 2952 (1995).
[17] J. Schweizer and M. P. Kennedy, Phys. Rev. E **52**, 4865 (1995).
[18] J. Alvarez-Ramirez, Phys. Rev. E **50**, 2339 (1994).
[19] J. L. Breeden, Phys. Lett. A **190**, 264 (1994).
[20] J. L. Breeden, F. Dinkelacker, and A. Hübler, Phys. Rev. A **42**, 5827 (1990).

[21] S. Fahy and D. R. Hamann, Phys. Rev. Lett. **69**, 761 (1992).
[22] Y.-Y. Chen, Phys. Rev. Lett. **77**, 4318 (1996).
[23] L. Molgedey, J. Schuchhardt, and H. G. Schuster, Phys. Rev. Lett. **69**, 3717 (1992).
[24] V. Hakim and W.-J. Rappel, Europhys. Lett. **27**, 637 (1994).
[25] A. Maritan and J. R. Banavar, Phys. Rev. Lett. **72**, 1451 (1994).
[26] L. M. Pecora and T. L. Caroll, Phys. Rev. Lett. **64**, 821 (1990).
[27] L. M. Pecora and T. L. Caroll, Phys. Rev. A **44**, 2374 (1991).
[28] Y. Liu and L. C. Barbosa, Phys. Lett. A **197**, 13 (1995).
[29] S. Varma and V. S. Varma, Phys. Rev. E **48**, 1670 (1993).
[30] A. Y. Loskutov and A. I. Shishmarev, Chaos **4**, 391 (1994).
[31] R.-R. Hsu, H.-T. Su, J.-L. Chern, and C.-C. Chen, Phys. Rev. Lett. **78**, 2936 (1997).
[32] J. Rössler, M. Kiwi, B. Hess, and M. Markus, Phys. Rev. A **39**, 5954 (1989).
[33] M. Lücke and Y. Saito, Phys. Lett. **91A**, 205 (1982).
[34] E. A. Jackson and A. Hübler, Physica D **44**, 407 (1990).
[35] V. V. Alekseev and A. Y. Loskutov, Dokl. Akad. Nauk (SSSR) **293** 1346 (1987) [Sov. Phys. Dokl. **32**, 270 (1987)].
[36] R. Lima and M. Pettini, Phys. Rev. A **41**, 726 (1990).
[37] Z. Qu, G. Hu, G. Yang, and G. Qin, Phys. Rev. Lett. **74**, 1736 (1995).
[38] Y. S. Kivshar, F. Rödelsperger, and H. Benner, Phys. Rev. E **49**, 319 (1994).
[39] L. Fronzoni, M. Giocondo, and M. Pettini, Phys. Rev. A **43**, 6483 (1991).
[40] Y. Braimin and I. Goldhirsch, Phys. Rev. Lett. **66**, 2545 (1991).
[41] R. Chacón, Phys. Rev. E **50**, 750 (1994).
[42] R. Meucci, W. Gadomski, M. Ciofini, and F. T. Arecchi, Phys. Rev. E **49**, 2528 (1994).
[43] J. Simonet, M. Warden, and E. Brun, Phys. Rev. E **50**, 3383 (1994).
[44] Y. Liu, N. Kikuchi, and J. Ohtsubo, Phys. Rev. E **51**, 2697 (1995).
[45] S. T. Vorha, L. Fabiny, and F. Bucholtz, Phys. Rev. Lett. **75**, 65 (1995).
[46] A. Azevedo and S. M. Rezende, Phys. Rev. Lett. **66**, 1342 (1991).
[47] H.-E. Sätherblom, Phys. Plasmas **4**, 174 (1997).
[48] W. X. Ding, H. Q. She, W. Huang, and C. X. Yu, Phys. Rev. Lett. **72**, 96 (1994).
[49] R. N. Dexter, D. W. Kerst, T. W. Lovell, S. C. Prager, and J. C. Sprott, Fusion Technol. **19**, 131 (1991).
[50] J. Kaplan and J. Yorke, in *Functional Differential Equations and the Approximation of Fixed Points*, edited by H. O. Peitgen and H. O. Walther, Lecture Notes in Mathematics Vol. 730 (Springer, Berlin, 1979), p. 204.
[51] P. Frederickson, J. Kaplan, and J. Yorke, J. Diff. Eqns. **49**, 185 (1983).
[52] A. Wolf, J. B. Swift, H. L. Swinney, and J. A. Vastano Physica D **16**, 285 (1985).
[53] T. Y. Li and J. A. Yorke, Am. Math. Monthly **82**, 985 (1975).
[54] R. C. Hilborn, *Chaos and Nonlinear Dynamics* (Oxford University Press, New York, 1994).
[55] M. Markus, Comput. Phys. **4**, 481 (1990).
[56] E. N. Lorenz, J. Atmos. Sci. **20**, 130 (1963).
[57] D. P. Lathrop and E. J. Kostelich, Phys. Rev. A **40**, 4028 (1989).
[58] E. N. Lorenz, in *Nonlinear Dynamics*, Ann. (N.Y.) Acad. Sci. **357**, 282 (1980), edited by R. H. G. Hellerman.
[59] J. Singer, Y.-Z. Wang, and H. H. Bau, Phys. Rev. Lett. **66**, 1123 (1991).
[60] O. E. Rössler, Phys. Lett. **57A**, 397 (1976).
[61] J. C. Sprott, Phys. Rev. E **50**, R647 (1994).
[62] J. C. Sprott, Phys. Lett. A **228**, 271 (1994).
[63] J. C. Sprott, Am. J. Phys. **65**, 537 (1997).
[64] N. M. Lawandy, D. V. Plant, and K. Lee, Phys. Rev. A **34**, 1247 (1986).
[65] W. V. R. Malkus, Mèm. Soc. R. Sci. Liège Collect. in-4 **IV**, 125 (1972).
[66] J. A. Yorke and E. D. Yorke, J. Stat. Phys. **21**, 263 (1979).
[67] S. H. Davis and M. N. Roppo, Physica D **24**, 226 (1987).
[68] E. A. Jackson and A. Kodogeorgiou, Phys. Lett. A **168**, 270 (1992).
[69] E. N. Lorenz, Nature (London) **353**, 241 (1991).
[70] T. Shinbrot, Adv. Phys. **44**, 73 (1995).
[71] W. Yang, M. Ding, A. J. Mandell, and E. Ott, Phys. Rev. E **51**, 102 (1994).
[72] D. Auerbach, Phys. Rev. Lett. **72**, 1184 (1994).
[73] H. G. Schuster and M. B. Stemmler, Phys. Rev. E **56**, 6410 (1997).
[74] R. O. Grigoriev, M. C. Cross, and H. G. Schuster, Phys. Rev. Lett. **79**, 2795 (1997).
[75] R. O. Grigoriev and M. C. Cross, Phys. Rev. E **57**, 1550 (1998).
[76] Z. Yoshida, Y. Sakuragi, and Y. Yamakoshi, J. Plasma Phys. **49**, 403 (1993).
[77] J. B. Taylor, Rev. Mod. Phys. **58**, 741 (1986).
[78] S. Assadi, S. C. Prager, and K. L. Sidikman, Phys. Rev. Lett. **69**, 281 (1992).
[79] A. B. Rechester and M. N. Rosenbluth, Phys. Rev. Lett. **40**, 38 (1978).
[80] C. A. Watts, D. E. Newman, and J. C. Sprott, Phys. Rev. E **49**, 2291 (1994).
[81] J. Stavans, F. Heslot, and A. Libchaber, Phys. Rev. Lett. **55**, 596 (1985).